INTERMOLECULAR INTERACTIONS IN SOLID BENZENE

G. J. Kearley[a], M. R. Johnson[b] and J. Tomkinson[c]

[a] *Department of Radiation, Radionuclides & Reactors,*

Faculty of Applied Sciences, Delft University of Technology,

Mekelweg 15, 2629 JB Delft, The Netherlands.

[b] *Institut Laue-Langevin (ILL), BP 156, 38042 Grenoble, Cedex 9, France*

[c] *CCLRC, The ISIS Facility, Rutherford Appleton Laboratory, CHILTON,*

OX11 0QX, UK

Abstract.

The lattice dynamics and molecular vibrations of benzene and deuterated benzene crystals are calculated from force-constants derived from density functional theory (DFT) calculations and compared with measured inelastic neutron scattering spectra. A very small change (0.5%) in lattice parameter is required to obtain real lattice-mode frequencies across the Brillouin zone. There is strong coupling between wagging and breathing modes away from the zone center. This coupling and sensitivity to cell-size arises from two basic interactions. Firstly, comparatively strong interactions that hold the benzene molecules together in layers. These include an intermolecular interaction in which H-atoms of one molecule link to the center of the aromatic ring of a neighboring molecule. The layers are held to each other by weaker interactions, which also have components that hold molecules together within a layer. Small changes in the lattice parameters change this second type of interaction and account for the changes to the lattice dynamics. The calculations also reveal a small auxetic effect in that elongation of the crystal along the c-axis, leads to an increase in internal pressure in the ac plane, that is elongation in the b direction induces expansion in the a and c directions.

Introduction.

Benzene is generally regarded as the prototypical example of an aromatic molecule and in the solid state it provides the simplest real system in which interactions between aromatic molecules can be studied. The aim of the present work is to understand the intermolecular interactions at a microscopic level that lead to molecular packing, lattice dynamics, phase behavior and ultimately the possibility of new bulk properties in aromatic systems. Over the years there have been a number of studies that are pertinent to this work: crystal structure [1], phases [2,3], and vibrational spectra [4-9], from both the experimental and theoretical standpoints.

The present work is mainly concerned with the calculation of intermolecular interactions using density functional methods (DFT), but in order to connect with experiment we compare our calculations not only with existing crystallographic data and optical vibrational spectroscopies, but also with new inelastic neutron scattering (INS) spectroscopy data. In this way we establish an almost parameter-free model that is capable of reproducing the static and dynamic structure factors. The use of DFT methods for periodic systems for the determination of molecular vibrations and zone center (Γ point) lattice modes, and comparison of these with INS spectra, has become common place in recent years [10,11]. Here these methods are extended to full lattice dynamics

calculations, taking into account the whole Brillouin zone. Increasingly, these calculations are being used to simulate not only the coherent inelastic neutrons scattering (INS) spectra from single crystals [12-14], but also the incoherent INS spectra of powdered samples. The latter is a far more straightforward experimental technique and alleviates the need for large single crystals of deuterated materials in the study of lattice dynamics.

Having established a model that reproduces the experimental data we shall exploit it to discern three major intermolecular interactions that hold the crystal together. One of these interactions is between the H-atom of one molecule with the center of the aromatic ring of a neighboring molecule. Clearly, this is unique to aromatic systems and it is important to establish the relative strength of this interaction by comparing simulation and experiment, mainly lattice dynamics in this case, and by investigating the effects of uniaxial and isotropic pressure in the simulation.

Experimental.

Benzene and deuterated benzene were obtained from The Aldrich Chemical Company and used without further purification. Samples were loaded in aluminum sample containers and cooled to 15K using a standard cryostat. Data were collected using the now defunct TFXA spectrometer (replaced with TOSCA) [15] at the ISIS pulsed neutron facility in the UK. Raw data were transformed into $S(\mathbf{Q}, \omega)$ using standard algorithms.

Crystallographic information

In a DFT calculation of solid state structure and dynamics of a molecular crystal, the only input is the measured crystal structure. For benzene, the structure has been determined at 4.2K to be orthorhombic in the space group Pbca, the unit cell and its contents being illustrated in figure 1. The cell parameters are a=7.355, b=9.371 and c=6.700 Å [1].

Computational Methods.

Energy calculations and structural optimization were made using VASP4.5 [16], using the PBE exchange-correlation functional and PAW pseudo-potentials with an energy cutoff of 600eV. A single crystallographic unit cell was used for all calculations, with the reciprocal lattice being sampled using 8 k-points (=[2,2,2]), Single-point energy calculations were made for a series of structures in which the crystallographically distinct atoms were displaced by 0.03Å in positive and negative directions along the x y and z directions. These calculations gave the Hellmann-Feynmann (HF) forces acting on each atom and were used as input for the lattice-dynamics program, PHONON4.2.4 [17]. Non-zero force constants were determined using the single unit cell, and it was found that all of these decayed by more than 3 orders of magnitude in going from the cell center to the nearest cell boundary. Phonon was used to calculate the eigenfrequencies, dispersion curves and simulated inelastic neutron scattering spectra, $S(\mathbf{Q},\omega)$. The

same HF forces were used for both C_6H_6 and C_6D_6, but the appropriate atomic masses and scattering crossections were used in the lattice dynamics calculations..

Results and Discussion.

Energy minimization, unit-cell optimization.

The first step in vibrational analysis is the optimization of the crystal structure so that the total energy is a minimum and the forces acting on the atoms are zero. However, optimization of the unit-cell parameters of weakly bound molecular crystals using DFT is not straightforward because long-range attractive interactions due to mutually induced dipoles cannot, in principle, be built into a theory based on one-electron density such as DFT using LDA and GGA exchange-correlation functionals. The fact that the dispersive interactions extend over the spatial range from ~3Å to ~8Å gives rise to a smoothly varying energy variation within the cell that can be considered in terms of a mean field.

This reasoning underlies the correction applied here in which the unit-cell parameters are constrained to experimental (or other) values in order to prevent unphysical cell expansion. For the present type of work, this is the only practical approach to the problem. Where dispersion has been calculated in other cases [8,9] the approach has been found to work reasonably well. A more direct test of this correction is the calculation of weak rotational potentials for methyl groups, which depend significantly on VdW interactions and are obtained with a precision

of ~90%, see for example ref. 18. which does not include non-local, long range correlation effects like dispersive interactions. In the present work this is crucial since we will show that rather small changes to the unit-cell parameters have important effects on the lattice dynamics. At worst, this can be conceived as 3 adjustable parameters: the pressure along each of the crystallographic directions. This means that the calculated variation of properties as a function of pressure will be incorrect by a constant factor that will be rather close to unity, but that the trends will be correct.

The starting model was taken from the most recent crystal structure determination (4.2K) [1], the atomic positions being relaxed, but with the unit-cell parameters being held constant. A lattice dynamics calculation using the optimized structure resulted in dispersion curves illustrated in figure 2. It is immediately clear from this figure that the acoustic modes and one of the optic modes become imaginary around the Y(0,1/2,0), S (1/2,1/2,0) and T (0,1/2,1/2). Whilst this may at first seem to be consistent with the proposal that this structure of benzene is only entropically stable [2], as we will show later, the lattice-mode INS spectrum calculated with this structure is in poor agreement with that measured.

As alluded to above, there is a small uncertainty in the unit-cell parameters due to the shortcoming of the current DFT method, and consequently we investigated the effects of slight scaling of the unit-cell parameters. A number of calculations were made using larger and smaller unit-cells and it transpired that

reducing the unit cell parameters (0.5 – 2.0%) had little effect on the dispersion curves, whilst increasing the cell parameters by as little as 0.5% (~0.04Å) removed all imaginary frequencies with the exception of some very small values for the acoustic modes at the Γ-point, k=0. The dispersion curves for the low-energy region of the smaller unit cell are illustrated in figure 3, and the observed and calculated INS spectra are shown in figure 4.

Molecular and lattice vibrations

We will denote the crystallographically determined unit cell as I and the 0.5% enlarged cell as II. A comparison of figures 2 and 3 reveals considerably different lattice dynamics for such a small change in unit-cell size, without change of symmetry. The inset in figure 4 compares the observed and calculated INS spectra in the lattice-mode region for cell I and cell II, which clearly reveals lost spectral density of the acoustic modes in the experimental cell, with an almost complete absence of intensity in the region around 40cm^{-1}. In addition the cell-I calculation does not show a Debye type spectrum in the limit ω->0. Whilst the agreement between the observed spectrum and the spectrum from cell II is not perfect in this region, it is a vast improvement for such a small change in lattice parameters.

Agreement between the observed and calculated spectra of the internal modes is rather good (figure 4) and is similar for either unit cell because these modes are much less sensitive to weak intermolecular interactions. Observed and calculated

spectra for C_6D_6 are shown in figure 5, and again it was found that cell II was required to avoid imaginary frequencies, and to give good agreement in the low-energy part of the spectrum. Formal assignments of all modes for both isotopomers are given in table 1. Assignments for the calculated frequencies in this table are based on the eigenvectors, and comparison with experimental values is based on symmetry species where possible, otherwise, best match.

Dispersion for the internal modes is generally less than about 15cm-1, with notable exception of the 1000cm^{-1} region. This spectral region, between 980 and 1010 cm^{-1}, is rather complicated because 12 crystal modes exist, arising from the three molecular modes: ring breathing, ν_1, H-wagging, ν_5, and in plane ring deformation, ν_{12}, these modes (and the proximate ν_{17}) being illustrated in figure 6. Dispersion of these modes is illustrated in figures 7 and 8 for cells II and I, respectively. We will first consider first the larger cell, II. A comparison of figures 7a and 7b shows that the ν_{17} wagging modes, between 960 and 980 cm^{-1} at the zone center, are essentially H-atom displacements over the whole zone. This consistent behavior across the zone is found for all modes except ν_1, ν_5 and ν_{12}, which mix strongly with each other at different wavevectors as is evident from figures 7a and 7b between 980 and 1010 cm^{-1}. Away from the zone center, the displacements in these modes are clearly a mixture of the formal molecular modes: ring breathing (symmetric and antisymmetric) with the out of plane wagging modes. The situation for the smaller cell, I, is markedly different (figure 8a and 8b). Not only is the dispersion in this region more pronounced, but here

the higher-frequency components of ν_{17} also mix with ν_1, ν_5 and ν_{12} away from the zone center.

This mixing of out-of-plane H-wagging modes with in-plane ring breathing modes away from the zone center suggests a significant intermolecular interaction between the H-atoms of one molecule and the aromatic core of the neighboring molecule, see below. The molecular center-of-mass displacement of these modes also varies across the zone due to the coupling of these internal modes with the lattice modes.

Intermolecular Interactions.

The crystal structure of benzene illustrated in figure 1 is conveniently regarded as composed of layers of molecules stacked along the long, b, axis, the molecules in each ac-layer are tilted by about 38^o to b. Inspection of the crystal structure reveals the 3 types of interaction that are illustrated in figure 9. The interactions labeled A and B are between the layers, whilst the layers themselves are held together by interaction D, and a more unusual type of interaction between the H-atoms and the aromatic rings of neighboring molecules, labeled C. In this interaction, the distance from the H-atom to each C-atom of the neighboring ring is almost the same, varying from 3.015 to 3.061Å, the distance from the H-atom to the center of the ring (labeled E) being only 2.701Å.

These interactions are examined in more detail in figure 10, where the electron density isosurface has been calculated at three different values. At the isosurface

0.045e the beginning of interaction type C can be seen between the two lower molecules, but the H-aromatic link has not actually been made. Looking at lower electron density, 0.035, the interaction type D is established but there is no actual link between the upper and lower molecules, and the H-aromatic link is still missing. Finally, at the isosurface 0.025e, all links are established, but it is interesting to note that the greatest overlap is by a combination of interactions C and D, which effectively merge the densities of the two lower molecules. The picture that emerges from this electron-density figure is of molecules that are held together in layers (lower molecules) by a quite strong interaction plus the H-aromatic interactions. The layers are linked to each other by weaker interactions. This picture is broadly consistent with the pattern of acoustic modes in figures 2 and 3, where the lowest energy mode is translation along Y, whilst the corresponding modes for X and Z are generally about 50% higher.

The anisotropy of the mean square displacements, collected in table 2, are also in agreement with this picture. Considering the H-atom involved in the H-aromatic interaction, C, displacement perpendicular to the approximate bond direction is noticeably larger than in the x-z plane. Similarly, H-atom interactions involved in connecting neighboring planes of molecules, along y, show less overall displacement in this direction. The overall isotropic values are in reasonable agreement with those measured crystallographically [1].

Auxetic effect of pressure along b-direction.

Intuitively we would expect the stronger interactions in the ac plane to be more sensitive to changes in the unit-cell size, but this is clearly not the case.

In order to proceed we have investigated the structural consequences on progressively changing the unit-cell b parameter. Figure 11 shows the results of these calculations starting from the parameters of cell II, and it can be seen that within the range on the b-parameters of cells I and II, there is a marked hardening of the cell along this direction. Perhaps more surprising is that in the range 1.002 to 0.996, the pressure along b increases by 3.1 kB, whilst the pressure along both a and c reduces by 0.7 kB. In terms of cell parameters, shortening b leads to compression along a and c, giving a negative Poisson's ratio, or auxetic behavior. This behavior can be understood by consideration of figures 1 and 9. The structural differences at the points 0.99 and 1.01 in figure 11 correspond to changes in C and D (figure 9), of only 0.002 Å this being consistent with the greater overlap of electron density shown on the right of figure 10. In contrast, distances A and B, between neighboring layers, decrease by 0.013 and 0.023 Å for compressing the b-direction from 1.01 to 1.00, but then increase by 0.040 and 0.016 Å, respectively, when compressing the b-direction further to 0.99. In order to establish the consistency of this effect we have also calculated the consequences of a 1% elongation of the cell along a. This leads to decreases in pressure along a and c of 1.9 and 1.2 kB, respectively, but an increase of 0.9 kB along b, this being entirely consistent with the results obtained above.

Without going into the fine detail of the rather small molecular reorientations, the basic scheme is as follows. It is important to notice that interactions A and B also have components in the ac plane so that initially, as the lattice is compressed along b interactions A and B increase pulling molecules in the ac plane together, reducing the pressure in this plane. Further compression (below ~0.998) forces the A and B interactions beyond their optimum allowing relaxation in the xz plane.

This pattern of interactions accounts for the high sensitivity of the acoustic modes at points: Y (0, ½, 0), S(½, ½, 0) and T(0, ½, ½) in the dispersion curves shown in figures 2 and 3. The b-parameter of cell I corresponds to 0.995 in figure 11, where the A and B interactions are not optimal, and hence at some points in the Brillouin zone y-displacements lead to an overall drop in the energy, and hence imaginary frequencies. When the A and B interactions are near optimal, all frequencies are real (apart from a very small error at k=0 for the acoustic modes) as seen in figure 3. This change in A and B interactions not only accounts for the changes in the dispersion of the lattice modes between cell I and cell II (figures 2 and 3), but also for the surprisingly large changes in the internal-mode dispersion of the H-wagging modes ν_5 and ν_{17}. Inspection of figures 1 and 6 reveals that all modes that wag the inter-layer hydrogens will strongly modulate the A and B (figure 9).

Conclusions.

DFT calculations are now sufficiently rapid and accurate to allow the vibrational dynamics of crystals such as benzene, and to verify these calculations against experimental spectroscopies. The principle difficulty is the uncertainty in dispersion energy, but this can be overcome by using pressure to constrain the lattice to the experimental values, effectively preventing physically unrealistic lattice expansion. In the case of benzene however, it is found that very small changes in unit-cell dimensions have a dramatic effect on the lattice dynamics and an expansion of only 0.5% above the experimentally determined values takes the cell from an unstable to a stable state. Although this leaves a small unknown scalar in the pressure, it is clear that the phonon dispersion, and the dispersion of some of the internal modes depend crucially on small changes to the lattice parameters.

The net interactions holding the molecules together in layers are stronger than those holding neighboring layers together. Because some interactions play both roles, forcing the layers together can increase the net interaction within the layers leading to a "contraction" of the layer. Changes in these interactions are entirely consistent with the sensitivity of the lattice modes and molecular vibrations to small changes in the unit-cell size. Constraining the unit cell parameters to values close to those experimentally determined is effectively a correction of the DFT method to take account of dispersive interactions. This has the consequence of introducing an offset in the pressure of about 10Kb, as seen in Figure 11. This will have some small effect on the relative values at which the

auxetic effect occurs, and it would be interesting to see if the predicted auxetic effect could be observed experimentally.

Dispersion of internal modes is normally only important where strong hydrogen bonding interactions are involved. In the present case there is significant intermolecular coupling of wagging and breathing modes of the aromatic ring that can be seen as Davidov splitting at the zone center, but which couples strongly to optic and acoustic phonons away from the zone center causing extensive mixing. This interaction is considerably stronger than would be suggested by an analysis of the optical spectra alone.

References

1. W. I. F. David, R. M. Ibberson, G. A. Jeffrey and J. R. Ruble, Physica B, 180 & 181 597 (1992)
2. P. Raiteri, R. Martoňák and M. Parrinello, Agnew. Chem. Int, 44, 2, (2005).
3. R. Martoňák, A. Laio, M. Bernasconi, C. Ceriani, P. Raiteri, F. Zipoli, and M. Parrinello, Z. Krist. 220 489 (2005).
4. H. Bonadeo, M. P. Marzocchi, E. Castellucci and S. Califano., J. Chem. Phys. **57**, 4299 (1972).
5. G. Taddei, H. Bonadeo, M. P. Marzocchi, and S. Califano., J. Chem. Phys. **58,** 966 (1973).
6. M. M. Thiéry and J. M. Léger, J. Chem. Phys., **89,** 4255 (1988).
7. M. M. Thiéry, J. M. Besson and J. L. Bribes, J. Chem. Phys., **96,** 2633 (1992).
8. M. R. Johnson and H. P. Trommsdorff, Chem. Phys. Lett., **364**, 34-38 (2002)
9. J. Stride, M. Adams and M. R. Johnson, Chem. Phys. (in press).
10. L. van Eijck, M. R. Johnson, G. J. Kearley, J. Phys. Chem. A.107, 8980 (2003)
11. M. Montejo, A. Navarro, G. J. Kearley, J. Vazquez, and J. J. Lopez-Gonzalez, J. Am. Chem. Soc. **126,** 15087-15095 (2004)

12. M. R. Johnson, K. Parlinski, I. Natkaniec and B. Hudson, Chem. Phys (2003) 291, 53;
13. P. Hermet, J.-L. Bantignies, A. Rahmani, J.-L. Sauvajol, M.R. Johnson and F. Serein, J. Phys. Cond. Matt. (2004) 16, 7385;
14. P. Hermet, J.-L. Bantignies, A. Rahmani, J.-L. Sauvajol and M.R. Johnson, J.Phys.Chem. A (2005) 109, 4202-4207
15. P. C. H. Mitchell, S. F. Parker, A. J. Ramirez-Cuesta and J. Tomkinson 'Vibrational Spectroscopy with Neutrons', World Scientific, New Jersey (2005)
16. G. Kresse, J. Furthmüller, Software VASP, Vienna (1999); G. Kresse, Phys. Rev. B 54 (11) (1996) 169; Comput. Mat. Sci. 6 (1996) 15.
17. K. Parlinski, Am. Inst. Phys. Conference Proceedings 479, "Neutrons and numerical methods N2M" Editors: M. R. Johnson, G. J. Kearley and H. G. Büttner, (1998).
18. M .R. Johnson, M. Prager, H. Grimm, M. A. Neumann, G. J. Kearley and C. C. Wilson, Chem. Phys **244**, 49 (1999)

Captions to tables.

Table 1.

Vibrational frequencies of crystalline benzene and deuterated benzene at the Γ-point (k=0). Observed frequencies are given in parenthesis: a=ref. 4, b=ref. 5, c=ref. 6, d=ref. 7. Calculated assignments and their symmetry species are based on the atomic displacements. R and I denote Raman and infrared active modes, respectively. Agreement with INS data is based on comparison of observed and calculated spectral profiles, figures 4 and 5.

Table 2.

Calculated mean square displacements for the crystallographically distinct atoms. The interaction type, a – d, are illustrated in figure 9. Figures in parentheses are for the H-atom after subtraction of the C-atom displacement.

Captions to figures.

Figure 1.

Schematic illustration of the crystal structure of C_6D_6 from ref.1 showing the relative orientation of molecules within the layers. The long b-axis is vertical.

Figure 2.

Dispersion curves in the low-frequency region for C_6H_6 using the experimentally determined [1] unit-cell parameters: a=7.355Å, b=9.371Å, c=6.700Å; cell-I. The negative values are used to indicate the magnitude of the imaginary frequencies.

Figure 3.

Dispersion curves in the low-frequency region for C_6H_6 using the bigger unit-cell parameters: a=7.397Å, b=9.422Å, c=6.737Å; cell-II. Notice the absence of negative (imaginary) values compared with figure 2.

Figure 4.

Observed (upper) and calculated (lower) INS profiles for C_6H_6 using the model cell-II. Calculation includes multiphonon modes up to 5 and convolution with an analytical instrumental resolution function. The inset shows the lattice mode region: observed (upper), cell-II (middle), cell-I (lower, dashed).

Figure 5.

Observed (upper) and calculated (lower) INS profiles for deuterated benzene, C_6D_6, using the model cell-II. Calculation includes multiphonon modes up to 5 and convolution with an analytical instrumental resolution function.

Figure 6.

Schematic illustration of the atomic displacements in the molecular modes that arise in the 960 to 1010 cm^{-1} spectral region (Γ-point).

Figure 7.

Mixing of formal molecular modes with each other and lattice modes across the zone. The behavior is not seen in other spectral regions.

a. Dispersion curves for cell-II in the region of ν_{17} (between 961 and 978 cm^{-1}), ν_5 (~990 and ~1005 cm^{-1}), ν_{12} (~992 and 996 cm^{-1}), and ν_1(~996 cm^{-1}), these frequencies being at the Γ-point, k=0. The density of the lines (grayscale) reflects the relative amplitude of the C-atom displacements.
b. As figure 7a, but the intensity of the lines (grayscale) represents the relative amplitude of the H-atom displacements.

Figure 8.

a. Dispersion curves for cell-II in the region of ν_{17}, ν_5, ν_{12}, and ν_1, to be compared with figure 7a. The intensity of the lines (grayscale) reflects the relative amplitude of the C-atom displacements.
b. As figure 8a, but the intensity of the lines (grayscale) represents the relative amplitude of the H-atom displacements.

Figure 9.

Illustration of the 3 major intermolecular interactions and their distances. The oval represents the center of the aromatic ring, the intermolecular distance to the nearest neighbor being E, 2.701Å. The orientation of this fragment is similar to that of the unit-cell in figure 1.

Figure 10.

Development of the electron density for interactions within the ac plane (lower molecules) and between planes (upper molecule), as the isosurface is decreased from 0.045e to 0.025e. Notice the large change in the H-aromatic overlap between 0.035e and 0.025e.

Figure 11.

Plot of calculated pressure in cell-II along each direction as a function of the fractional change in the lattice parameter c (for 1.000 c=6.737Å). The atomic positions were relaxed to the energy minimum for each value of c.

Table 1.

C_6H_6 (cm^{-1})	C_6D_6 (cm^{-1})	Assignment (crystal)	Molecular mode
-1	-1	B2u(l)	Lattice modes
-1	-1	B3u(l)	
0	0	B1u(l)	
55 (57[a])	50	Ag(R)	
56	54	Au	
57 (57 [a])	53	B1g(R)	
59 (61 [a]) (53 [b])	53 57	B3g(R)+B2u(l)	
64 (70 [b])	62	B1u(l)	
66	64	Au	
72 (79 [a])	66	Ag(R)	
74 (53 [b])	71	B3u(l)	
78 (79 [a])	71	B2g(R)	
80 (100 [a])	73	B1g(R)	
87 (90 [a])	79	B2g(R)	
89 (92 [a]) (94 [b])	81 86	Ag(R)+B3u(l)	
95 (92 [a])	86	B3g(R)	
98	95	Au	
102 (85[b])	93 95	B2g(R)+B1u(l)	
104 (94 [b])	101	B2u(l)	
126 (128 [a])	115	B3g(R)	
127 (128 [a])	117	B1g(R)	
397	345	B2u(l)+B3u(l)	ν_{16} E_{2u}
399 (401 [d])	347 (353 [d])	Au	
399 (404 [d])	348	Au+B1u(l)	

402 (405[d])	351	B2u(I)	
412	361	B3u(I)	
412	361 (364[d])	B1u(I)	
597	568	B2g(R)	ν_6 E_{2g}
598	570	Ag(R)	
598	571	B3g(R)	
600 (600[c])	571 572	Ag(R)+B1g(R)	
601	571	B1g(R)	
602	573	B2g(R)	
603 (606[c])	576	B3g(R)	
664	489	B3u(I)	ν_{11} A_{2u}
666 (685[d])	490 (515[d])	B1u(I)	
691 (674[d])	507 (506[d])	Au	
692 (690[d])	508 (525[d])	B2u(I)	
703	599	B3g(R)	ν_4 B_{2g}
703	600	B1g(R)	
707	609	B2g(R)	
708	611	Ag(R)	
838	653	Ag(R)	ν_{10} E_{1g}
839	653	B1g(R)	
842	656	Ag(R)	
847	660	B2g(R)	
850	662	B3g(R)	
853 (852[c])	665	B2g(R)	
866	671	B3g(R)	
867	672	B1g(R)	
961	784	B3u(I)	

962	784	B2u(I)	ν_{17} E_{2u}
963 (974 [d])	785 (795 [d])	Au	
966	788	B1u(I)	
967 (983 [d])	786 788	Au+B2u(I)	
977	792	B3u(I)	
978 (977 [d])	792 (799 [d])	B1u(I)	
988 (978[c])	823	B3g(R) ν_5	ν_1 A_{1g}
989 (983 [c])	823	B1g(R) ν_5	ν_5 B_{2g}
992	953	B3u(I) ν_{12}	ν_{12} B_{1u}
992 (1010 [d])	953 (970 [d])	B1u(I) ν_{12}	
993	954	B2u(I) ν_{12}	
995 (991 [c])	827 950	Ag(R) ν_1 + B1g(R) ν_1	
996 (997[c],1006 [d])	826 957 (967 [d])	B2g(R) ν_1 + Au ν_{12}	
997	952	B3g(R) ν_1	
1003	951	B2g(R) ν_5	
1006 (1006[c])	952	Ag(R) ν_5	
1031	801	B2u(I)	ν_{18} E_{1u}
1034	803	B1u(I)+B3u(I)	
1035 (1035[d])	803 (810 [d])	Au	
1036	807	Au	
1039 (1038 [d])	808 (814 [d])	B3u(I)	
1040	808	B1u(I)	
1041	810	B2u(I)	
1132	809	B3u(I)	

1134 (1142 [d])	810 (823 [d])	Au	ν_{15} B_{2u}
1138	813	B1u(I)	
1142	816	B2u(I)	
1154	844	Ag(R)	ν_9 E_{2g}
1159	849	B1g(R)	
1159	849	B2g(R)	
1160	849	B3g(R)	
1162 (1169 [c])	850	Ag(R)	
1163 (1174 [c])	853	B2g(R)	
1164 (1177 [c])	852	B3g(R)	
1169 (1181 [c])	857	B1g(R)	
1328	1036	B3g(R)	ν_3 A_{2g}
1330	1037	Ag(R)	
1332	1039	B1g(R)	
1334	1040	B2g(R)	
1346	1324	B3u(I)	ν_{14} B_{2u}
1348	1322	B1u(I)	
1348 (1312 [d])	1325 (1286 [d])	Au	
1349	1324	B2u(I)	
1459	1325	B1u(I)	ν_{19} E_{1u}
1461	1325	B2u(I)	
1463 (1470 [d])	1327 (1326 [d])	Au	
1463	1327	B3u(I)	
1463 (1478 [d])	1344	B2u(I)	
1465 (1475 [d])	1343 (1329 [d])	B1u(I)	
1467	1343	B3u(I)	
1468	1344	Au	

1588 (1585 [c])	1551 1552 1551	Ag(R)+B2g(R)+ B3g(R)	ν_8 E_{2g}
1589	1552 1553	B1g(R)+B3g(R)	
1590	1555	Ag(R)	
1590	1553	B2g(R)	
1592	1555	B1g(R)	
3100	2291	B1u(I)+B3u(I)	ν_{13} B_{1u}
3102	2292	Au	
3102	2293	B2u(I)	
3106 (3044 [c])	2298	B2g(R)	ν_7 E_{2g}
3107 (3048 [c])	2298 2299	Ag(R)+B1g(R)	
3107	2299	B3g(R)	
3111	2302	B2g(R)	
3111	2302	Ag(R)	
3112	2303	B3g(R)	
3113	2304	B1g(R)	
3117	2315	B2u(I)	ν_{20} E_{1u}
3118 (3033 [d])	2315 (2267 [d])	Au	
3118 (3038 [d])	2315 (2278 [d])	B1u(I)	
3119 (3088 [d])	2316	B3u(I)	
3125 (3069 [d])	2319 (2282 [d])	B2u(I)	
3125 (3092 [d])	2320	Au	
3126	2320	B1u(I)+B3u(I)	
3128 (3061 [c])	2327	B3g(R)	ν_2 A_{1g}
3130	2328	B1g(R)	
3131	2329	B2g(R)	
3131	2329	Ag(R)	

Table 2.

Atom interaction type	MSD-x (Å^2)	MSD-y (Å^2)	MSD-z (Å^2)	Isotropic (Å^2)
Ha	0.74 (0.52)	0.71 (0.54)	0.73 (0.53)	0.73 (0.53)
Hc	0.70 (0.51)	0.78 (0.57)	0.75 (0.54)	0.74 (0.54)
Hd	0.74 (0.52)	0.61 (0.50)	0.79 (0.55)	0.71 (0.52)
Ca	0.22	0.17	0.20	0.20
Cc	0.19	0.21	0.21	0.20
Cd	0.22	0.11	0.24	0.19

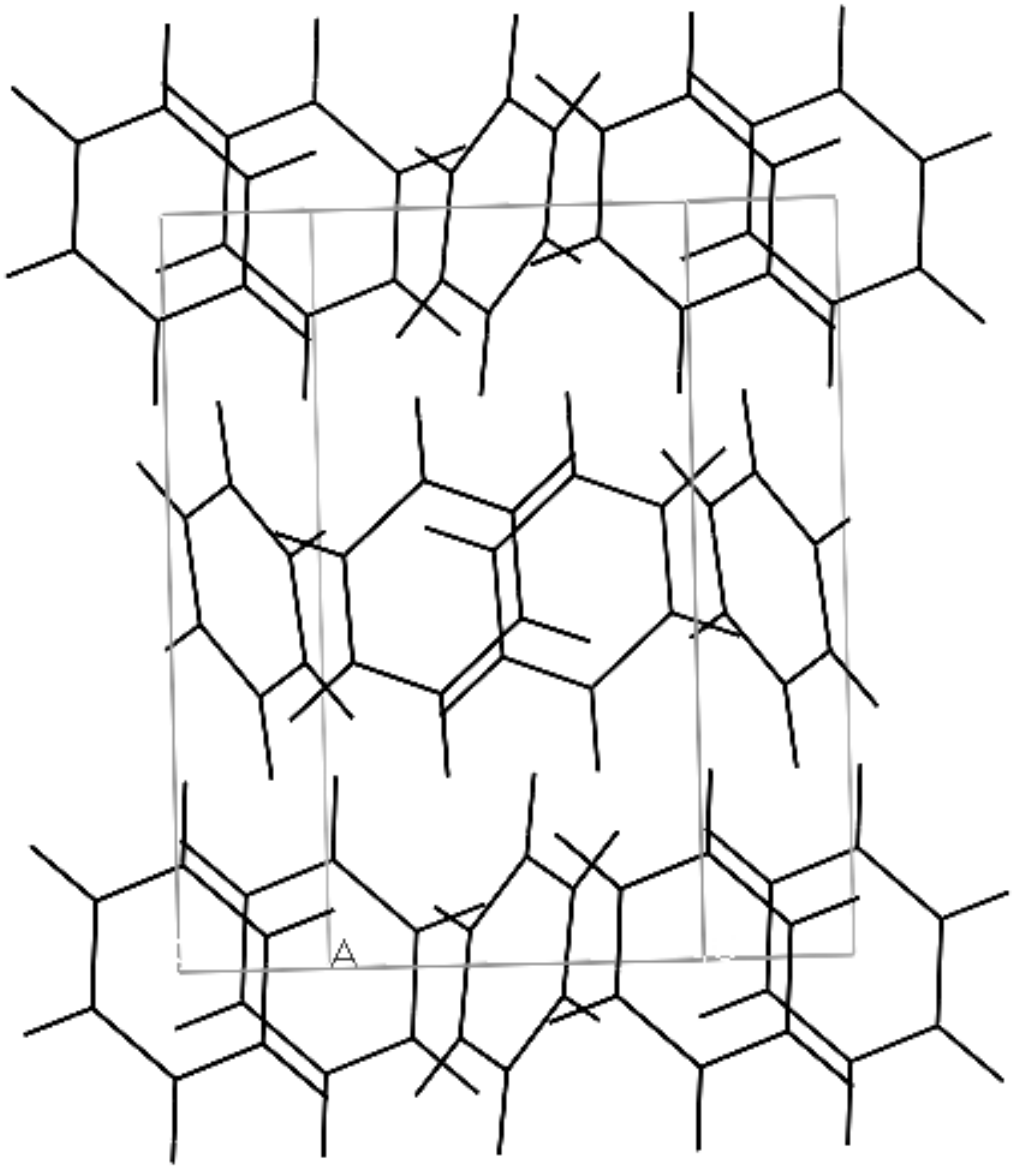

Fig. 1

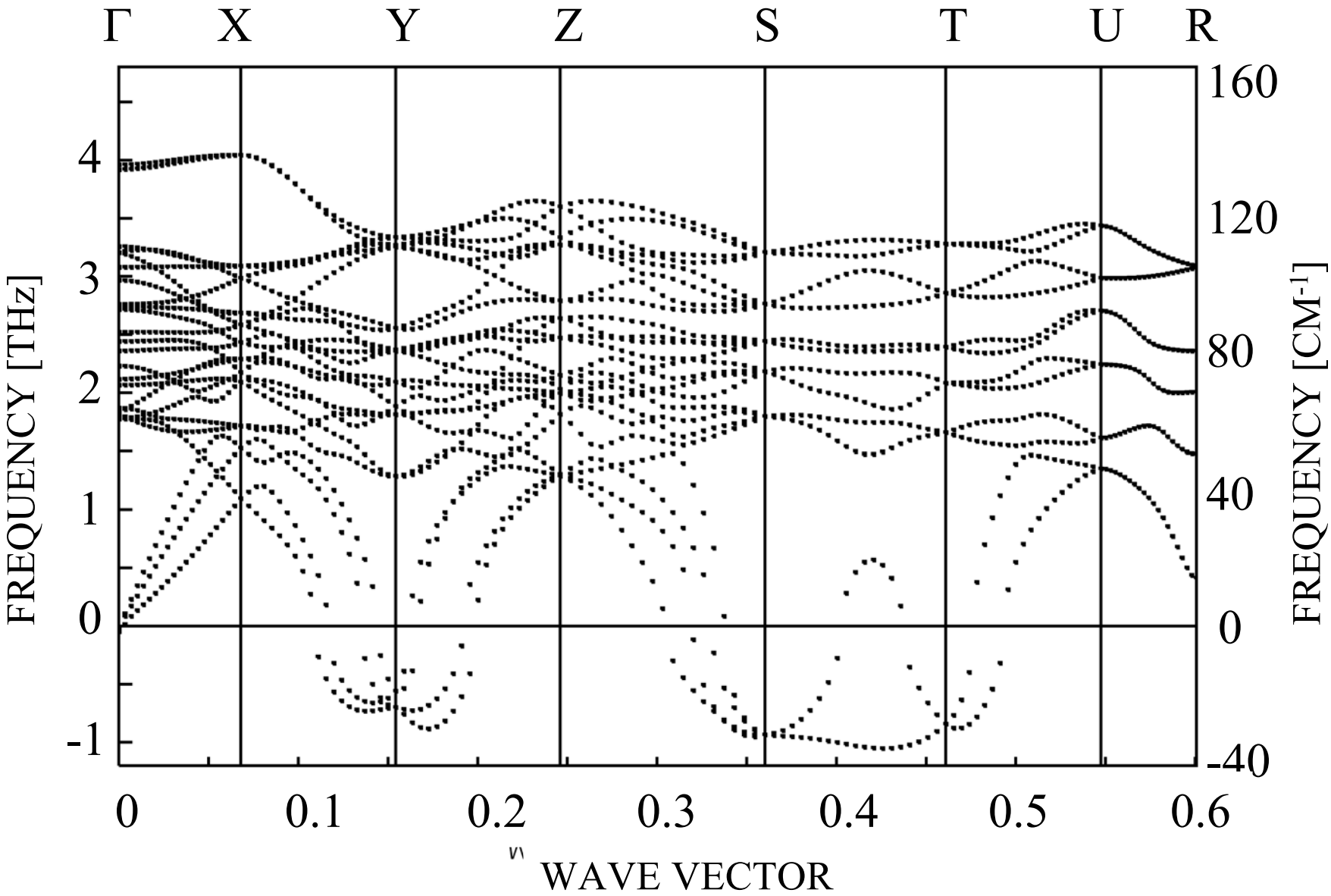
Γ
X
Y
Z
S
T
U
R
FREQUENCY [THz]
4
3
2
1
0
-1
160
120
80
40
0
-40
FREQUENCY [CM-1]
0
0.1
0.2
0.3
0.4
0.5
0.6
WAVE VECTOR

Fig. 2

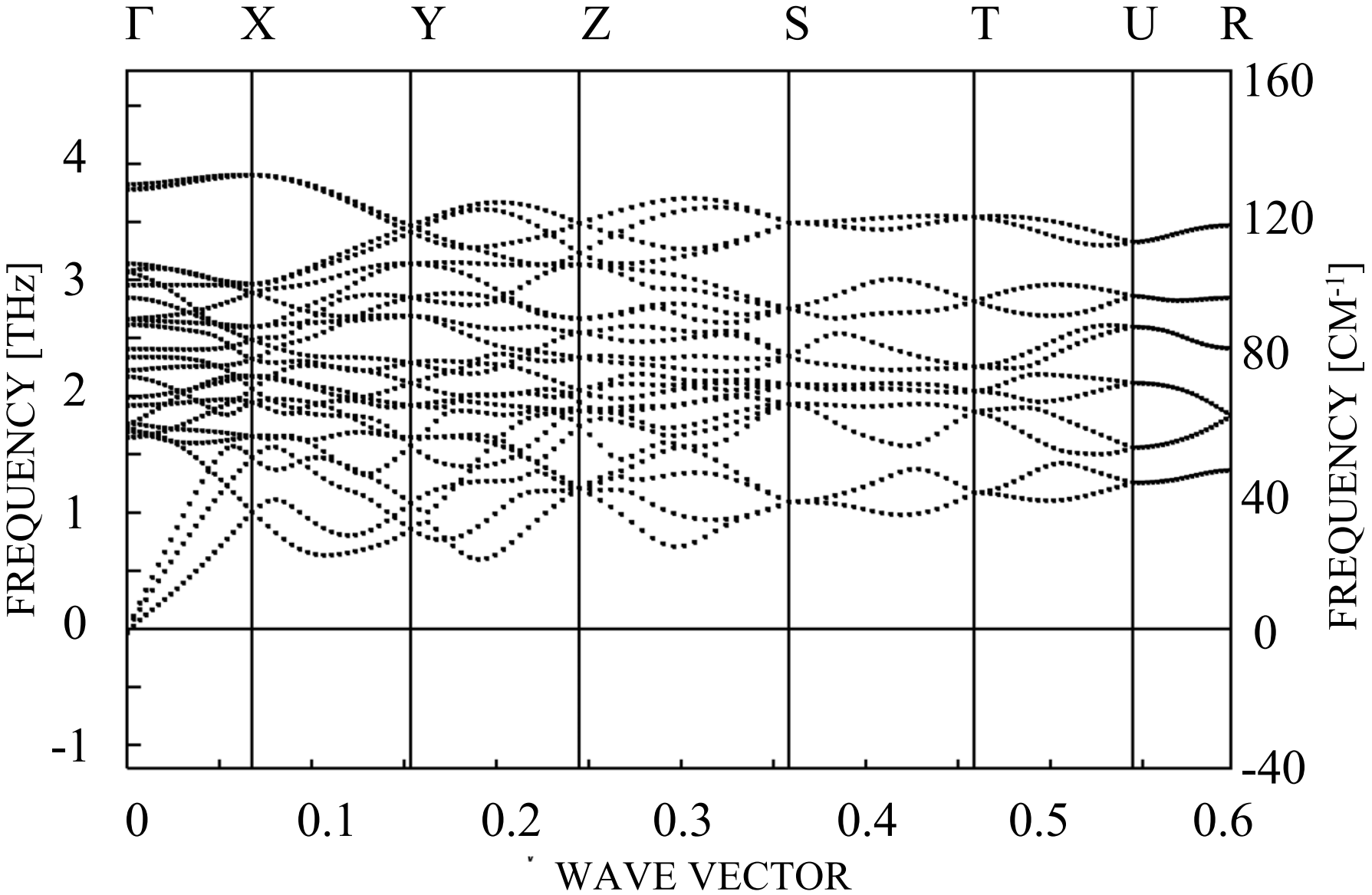
Γ
X
Y
Z
S
T
U
R
FREQUENCY [THz]
4
3
2
1
0
-1
FREQUENCY [CM-1]
160
120
80
40
0
-40
0
0.1
0.2
0.3
0.4
0.5
0.6
WAVE VECTOR

Fig. 3

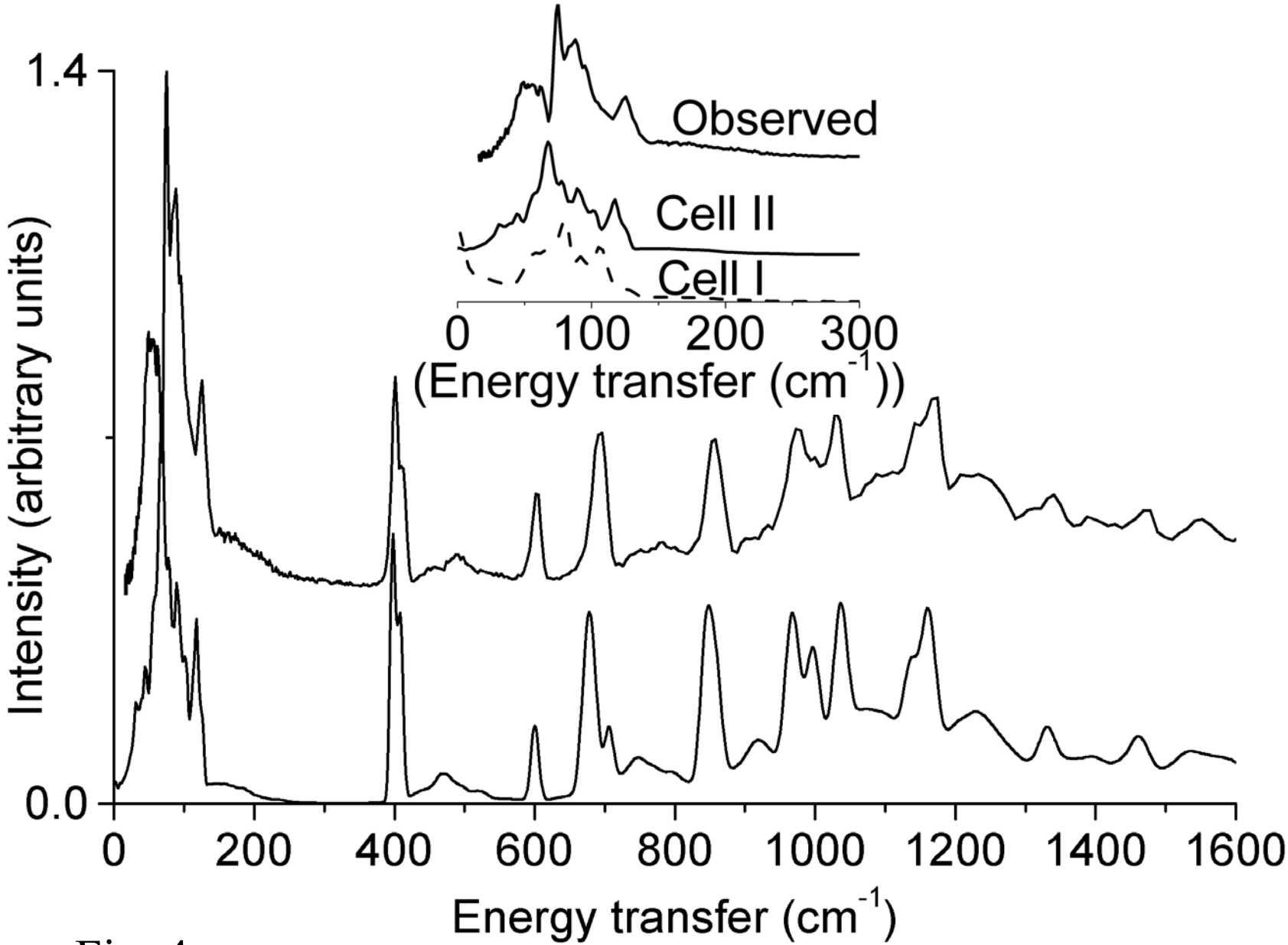
1.4
0.0
Intensity (arbitrary units)
0
200
400
600
800
1000
1200
1400
1600
Energy transfer (cm-1)
Observed
Cell II
Cell I
0
100
200
300
(Energy transfer (cm-1))

Fig. 4

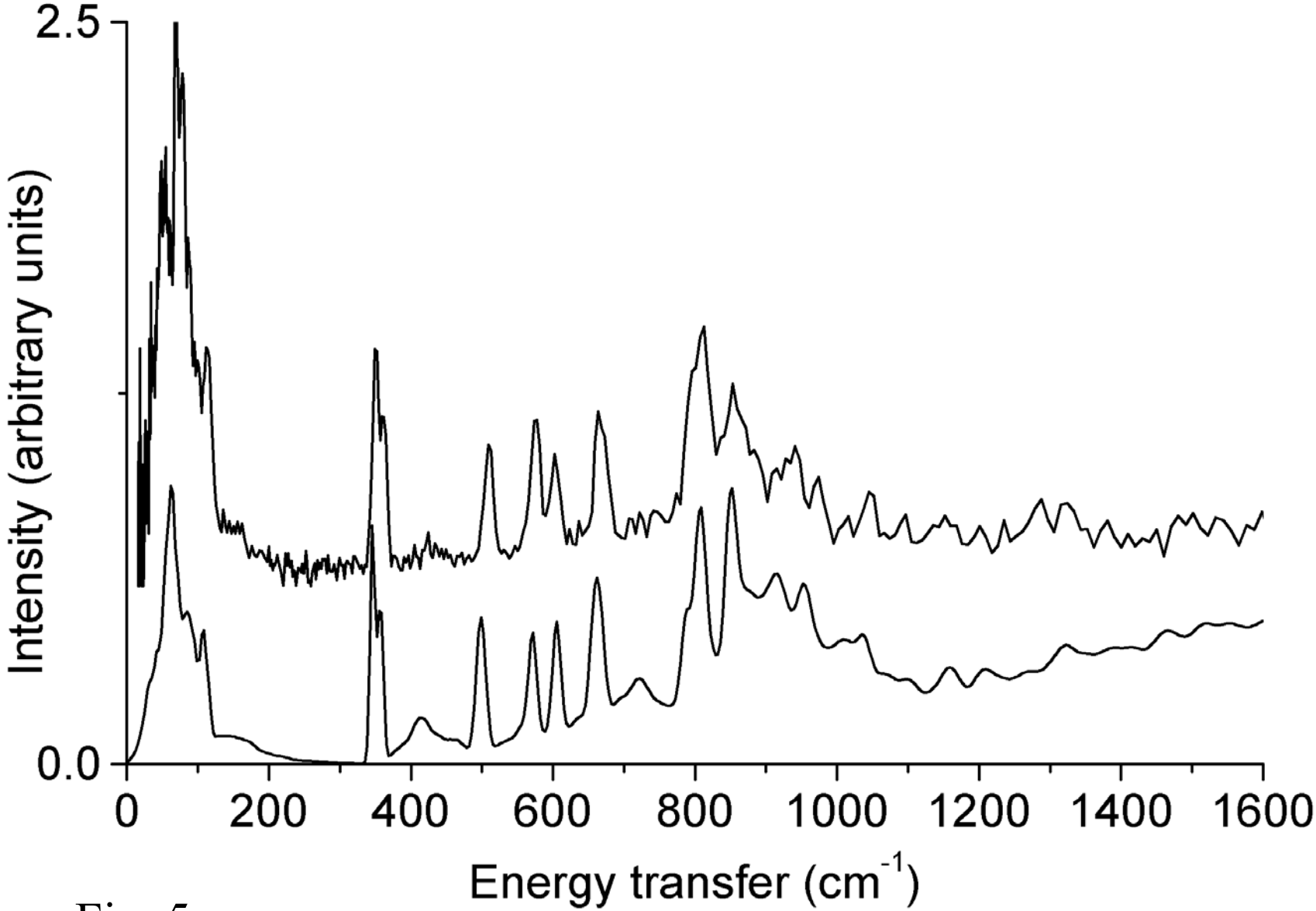
2.5
0.0
Intensity (arbitrary units)
0
200
400
600
800
1000
1200
1400
1600
Energy transfer (cm-1)

Fig. 5

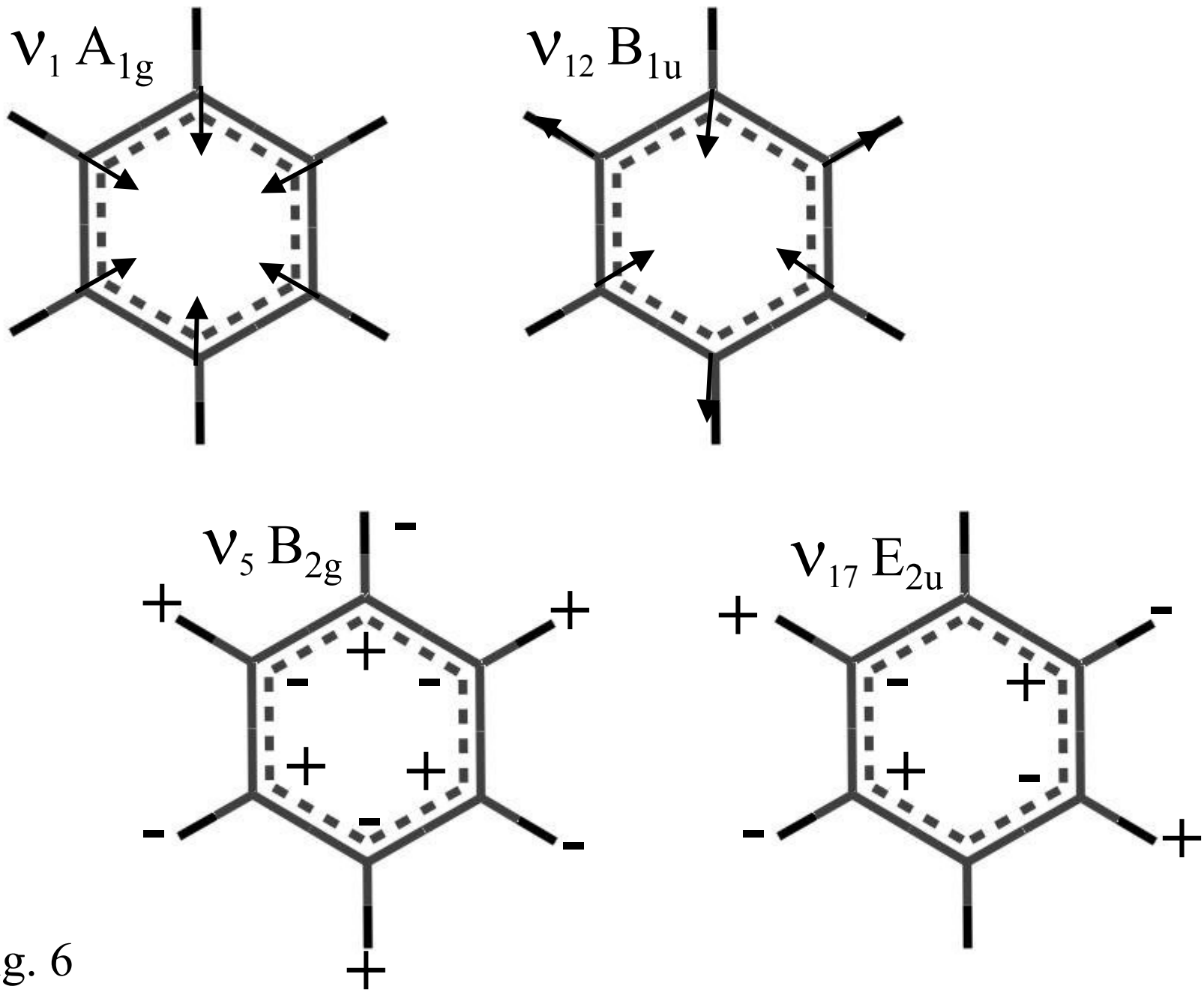

Fig. 6

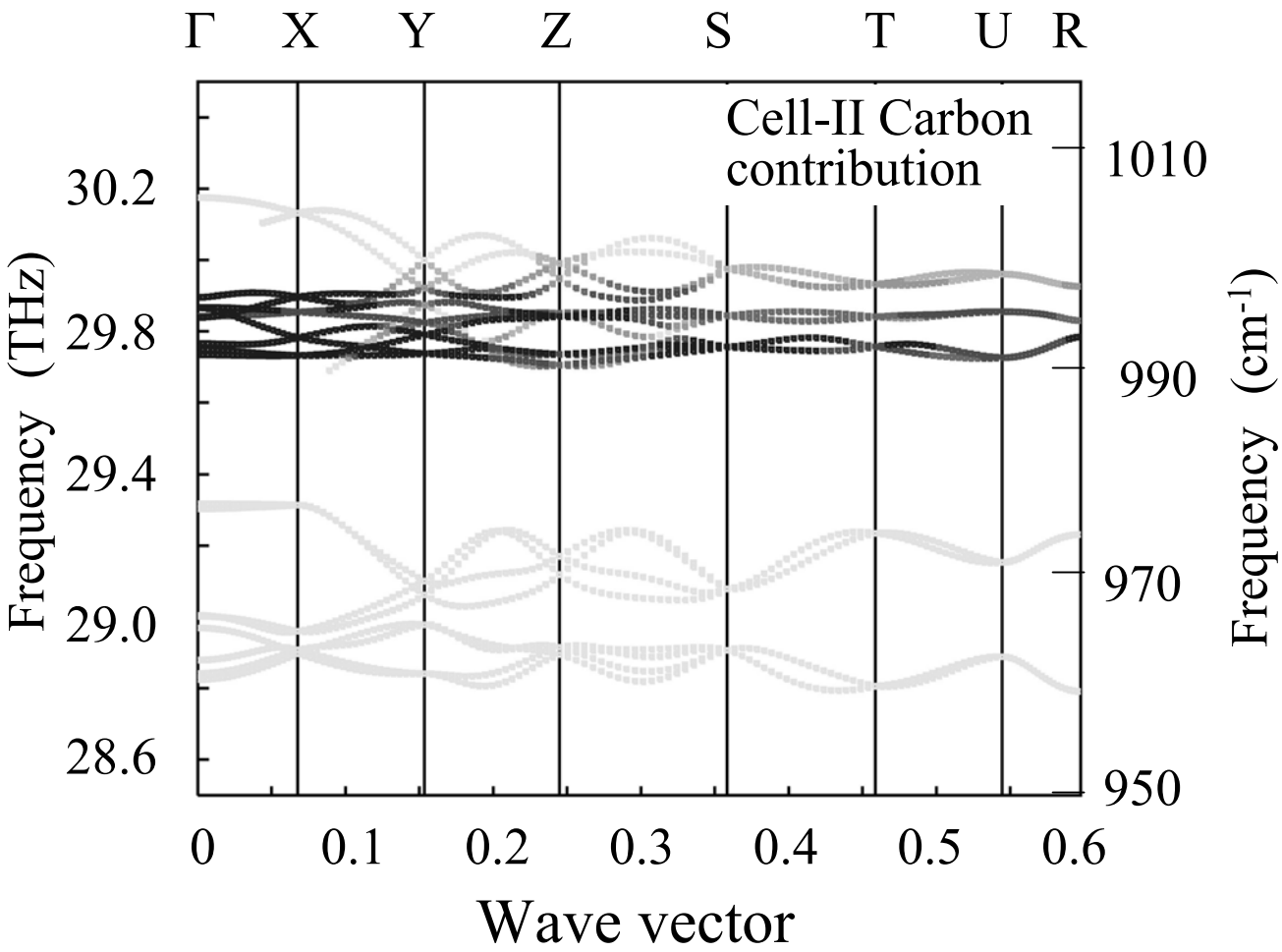
Γ X Y Z S T U R
Cell-II Carbon contribution
30.2
29.8
29.4
29.0
28.6
Frequency (THz)
1010
990
970
950
Frequency (cm-1)
0 0.1 0.2 0.3 0.4 0.5 0.6
Wave vector

Fig. 7a

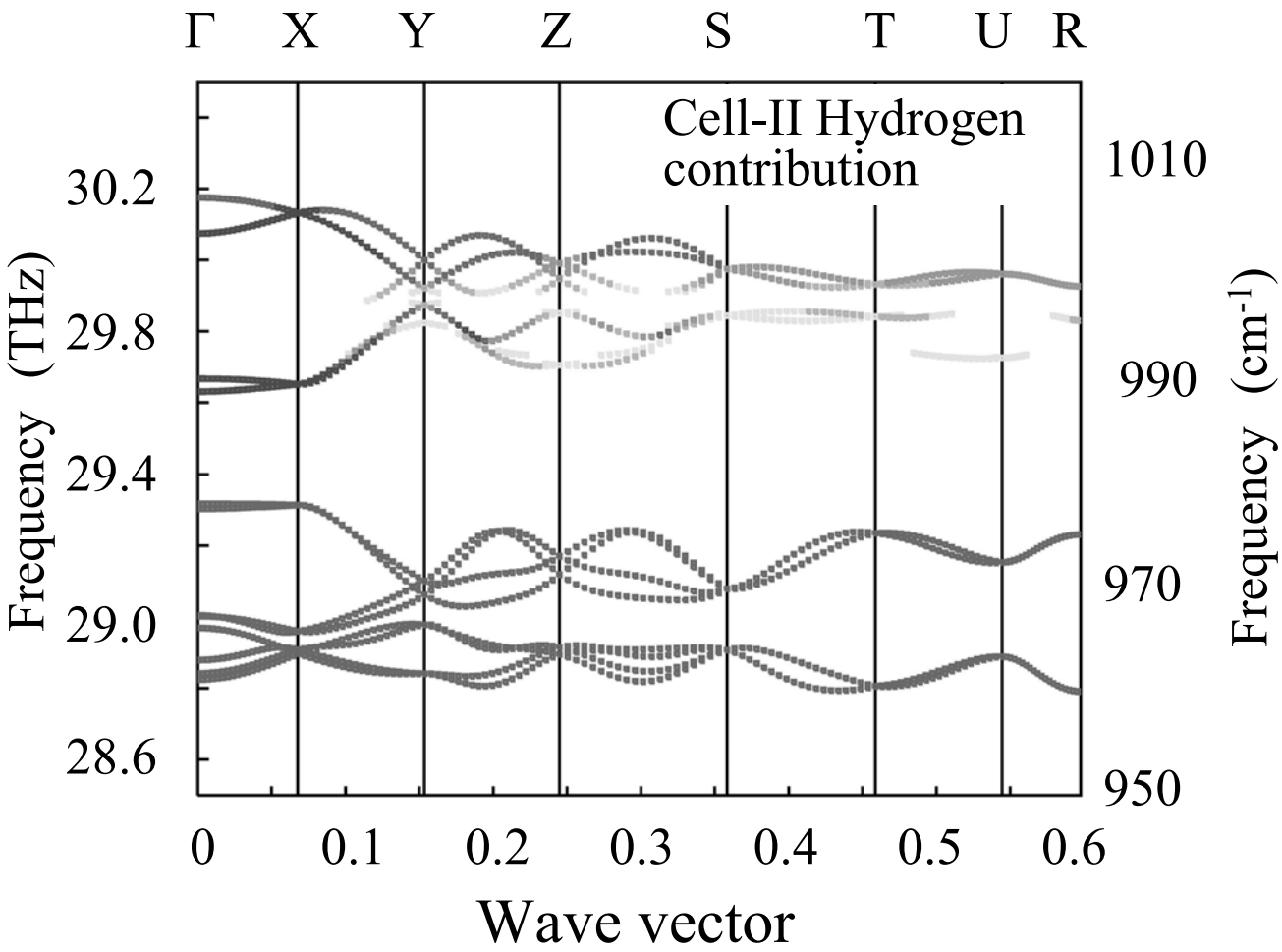
Γ X Y Z S T U R
Cell-II Hydrogen contribution
30.2
29.8
29.4
29.0
28.6
Frequency (THz)
1010
990
970
950
Frequency (cm-1)
0 0.1 0.2 0.3 0.4 0.5 0.6
Wave vector

Fig. 7b

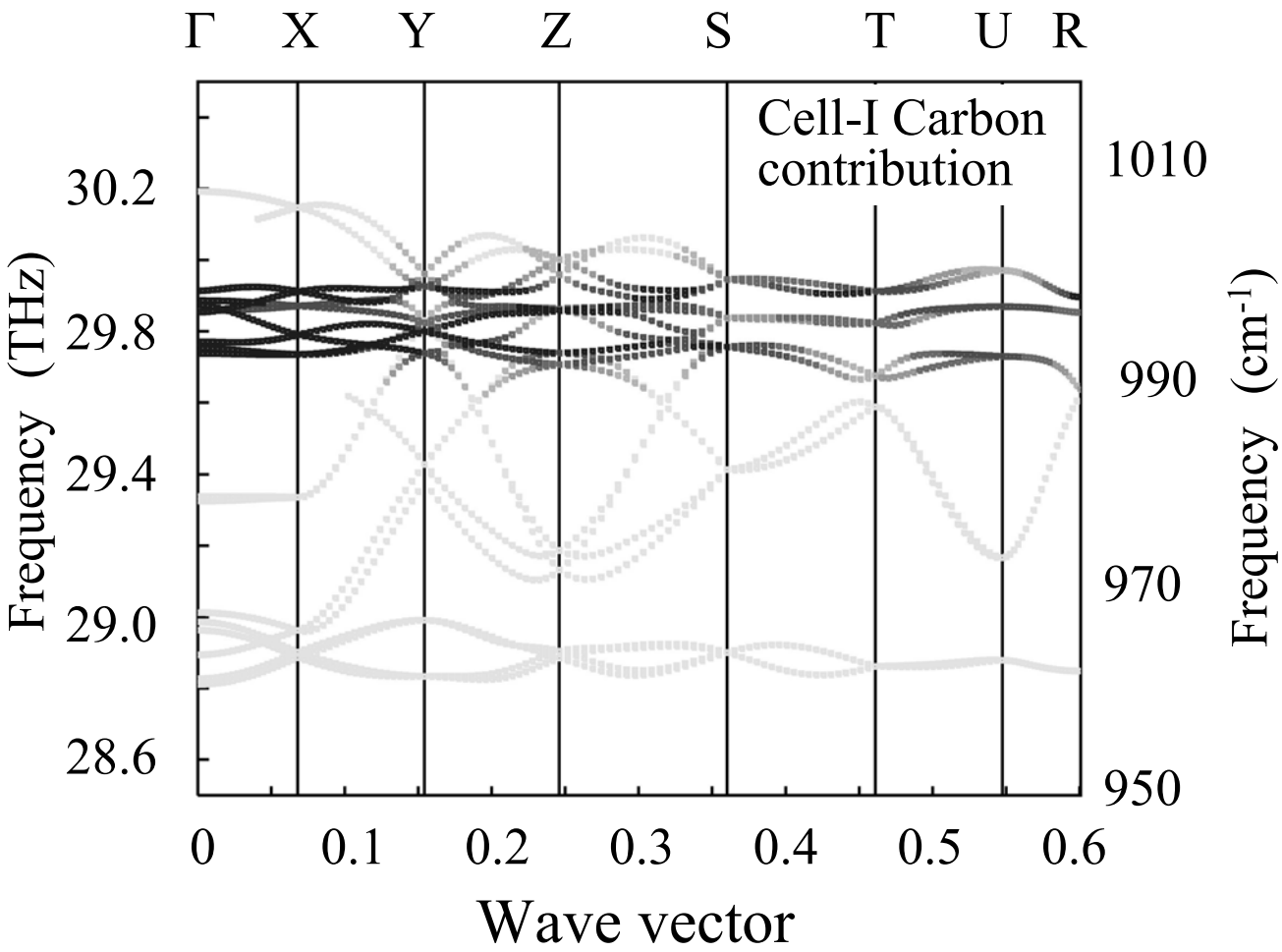
Γ X Y Z S T U R
Cell-I Carbon contribution
30.2
29.8
29.4
29.0
28.6
Frequency (THz)
1010
990
970
950
Frequency (cm-1)
0 0.1 0.2 0.3 0.4 0.5 0.6
Wave vector

Fig. 8a

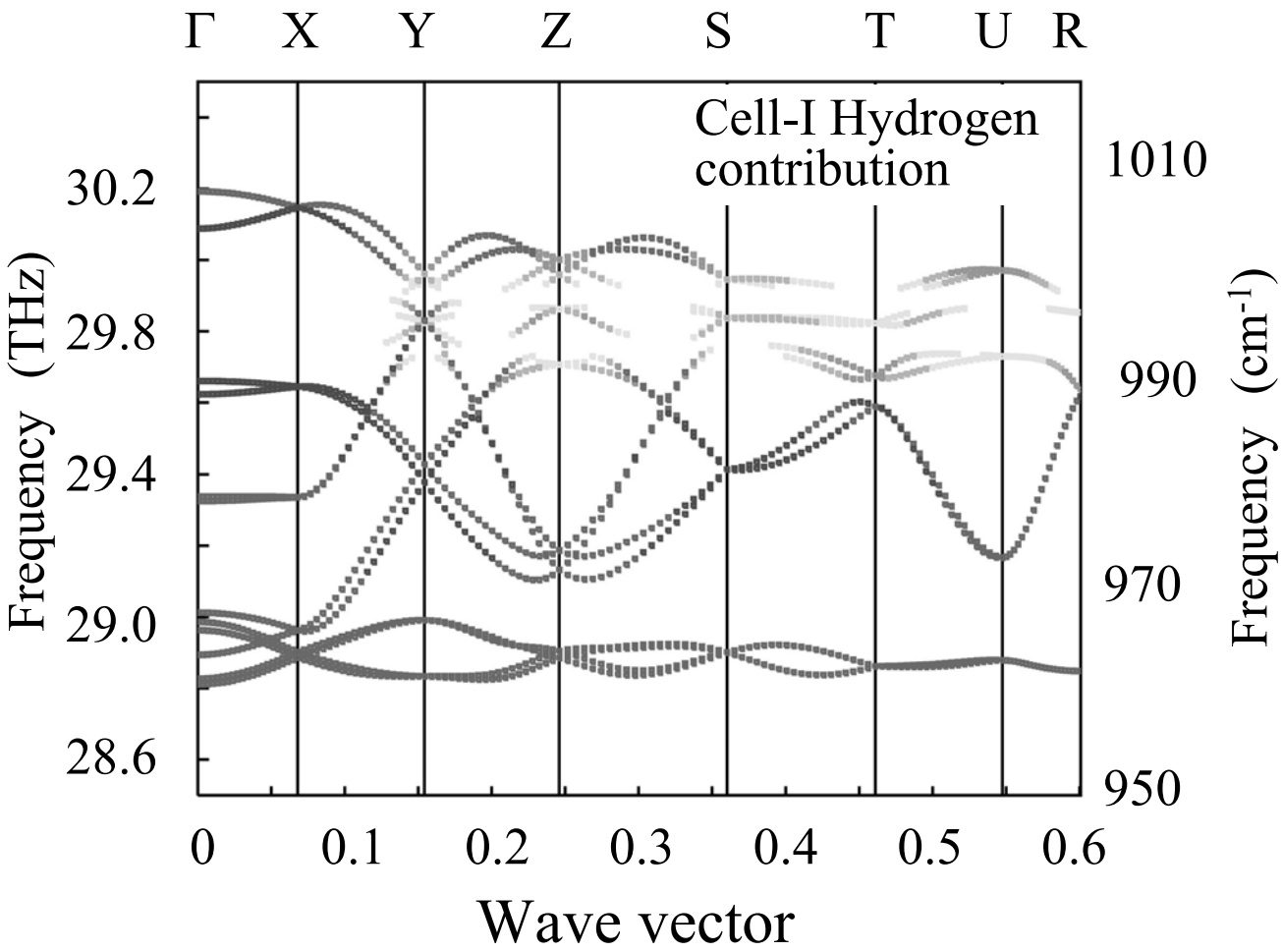
Γ X Y Z S T U R
Cell-I Hydrogen contribution
30.2
29.8
29.4
29.0
28.6
Frequency (THz)
1010
990
970
950
Frequency (cm-1)
0 0.1 0.2 0.3 0.4 0.5 0.6
Wave vector

Fig. 8b

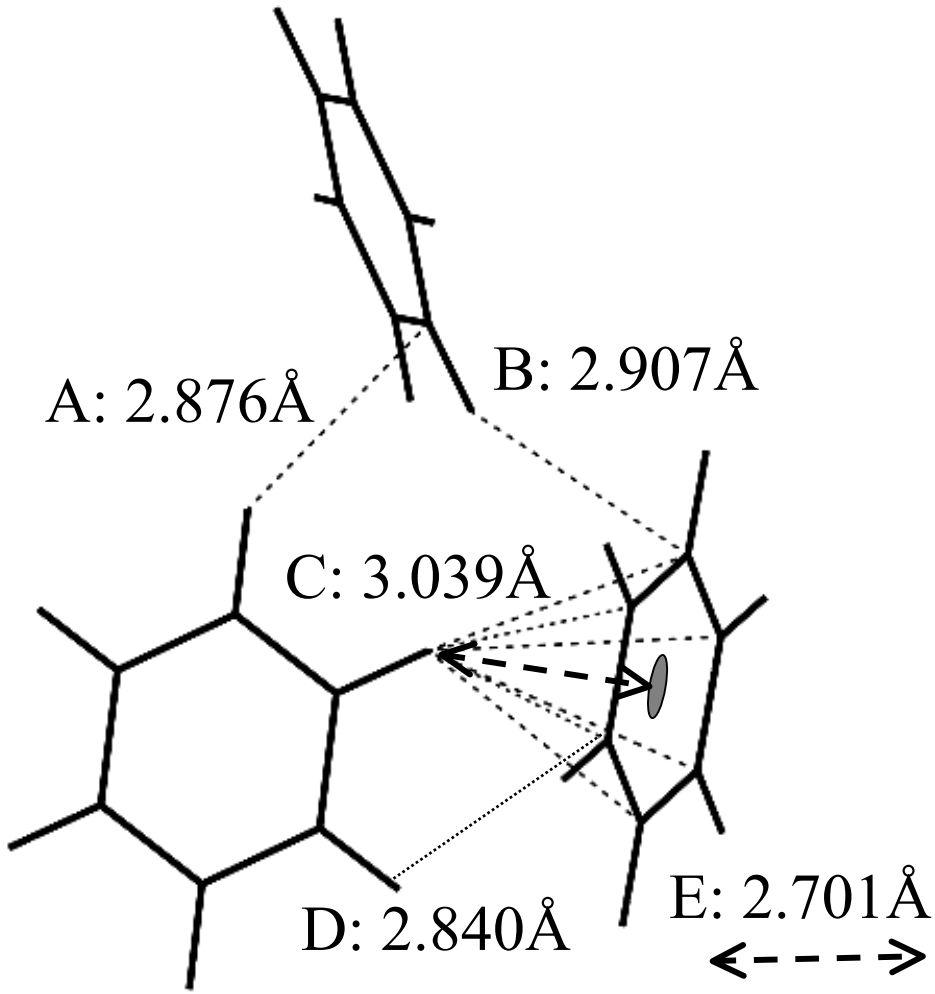

Fig. 9

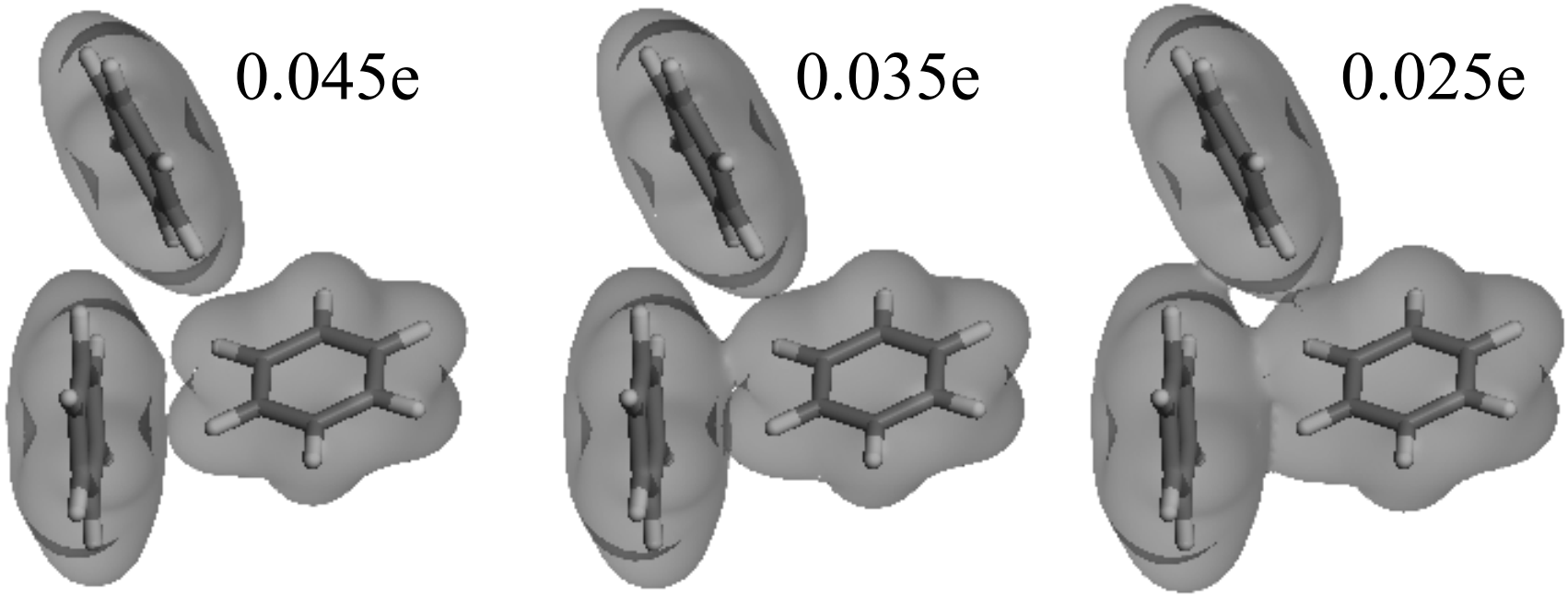

Fig. 10

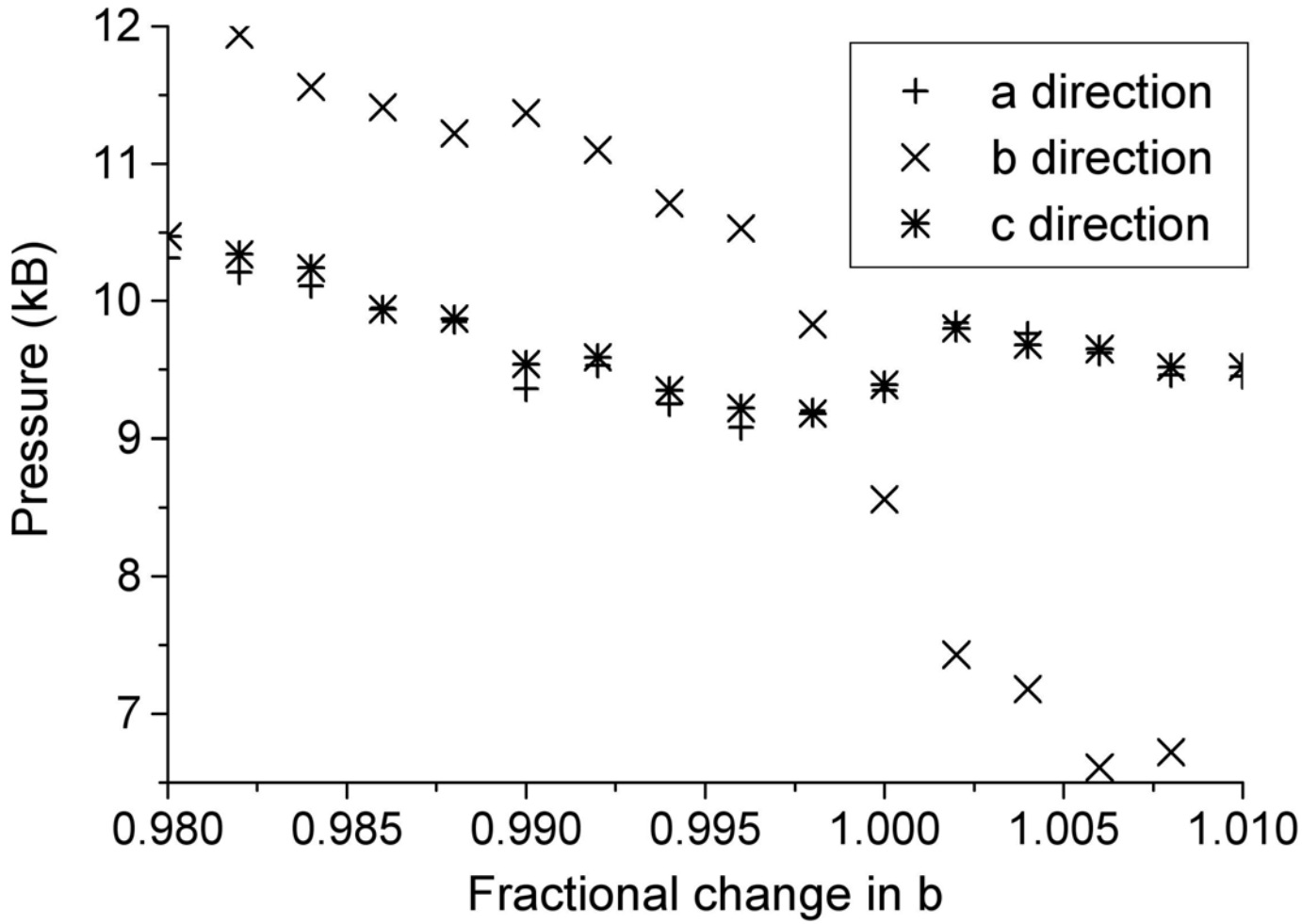
Pressure (kB)
12
11
10
9
8
7
0.980
0.985
0.990
0.995
1.000
1.005
1.010
Fractional change in b
a direction
b direction
c direction

Fig. 11